A simple model for the cloud adjacency effect and the apparent bluing of aerosols near clouds

Popular Summary

In determining aerosol-cloud interactions, the properties of aerosols must be characterized in the vicinity of clouds. Numerous studies based on satellite observations have reported that aerosol optical depths increase with increasing cloud cover. Part of the increase comes from the humidification and consequent growth of aerosol particles in the moist cloud environment, but part comes from 3D cloud-radiative transfer effects on the retrieved aerosol properties. Often, discerning whether the observed increases in aerosol optical depths are artifacts or real proves difficult. The paper provides a simple model that quantifies the enhanced illumination of cloud-free columns in the vicinity of clouds that are used in the aerosol retrievals. This model is based on the assumption that the enhancement in the cloud-free column radiance comes from enhanced Rayleigh scattering that results from the presence of the nearby clouds. The enhancement in Rayleigh scattering is estimated using a stochastic cloud model to obtain the radiative flux reflected by broken clouds and comparing this flux with that obtained with the molecules in the atmosphere causing extinction, but no scattering.

A simple model for the cloud adjacency effect and the apparent bluing of aerosols near clouds

Alexander Marshak[1], Guoyong Wen[2], James A. Coakley, Jr.[3], Lorraine A. Remer[1], Norman G. Loeb[4], and Robert F. Cahalan[1]

[1] NASA – Goddard Space Flight Center, Climate and Radiation Branch, MD
[2] University of Maryland Baltimore County, MD
[3] Oregon State University, OR
[4] NASA Langley Research Center, Climate Science Branch, Hampton, VA

Correspondence
Alexander Marshak
tel. 301-614-6122
email: Alexander.Marshak@nasa.gov

Prepared for publication in JGR
"Yoram J. Kaufman symposium on aerosols, clouds and climate" issue

A simple model for the cloud adjacency effect and the apparent bluing of aerosols near clouds

Abstract

In determining aerosol-cloud interactions, the properties of aerosols must be characterized in the vicinity of clouds. Numerous studies based on satellite observations have reported that aerosol optical depths increase with increasing cloud cover. Part of the increase comes from the humidification and consequent growth of aerosol particles in the moist cloud environment, but part comes from 3D cloud-radiative transfer effects on the retrieved aerosol properties. Often, discerning whether the observed increases in aerosol optical depths are artifacts or real proves difficult. The paper provides a simple model that quantifies the enhanced illumination of cloud-free columns in the vicinity of clouds that are used in the aerosol retrievals. This model is based on the assumption that the enhancement in the cloud-free column radiance comes from enhanced Rayleigh scattering that results from the presence of the nearby clouds. The enhancement in Rayleigh scattering is estimated using a stochastic cloud model to obtain the radiative flux reflected by broken clouds and comparing this flux with that obtained with the molecules in the atmosphere causing extinction, but no scattering.

1. Introduction

Numerous studies based on satellite observations have reported a positive correlation between cloud amount and aerosol optical thickness (AOT) (e.g., Sekiguchi et al., 2003; Loeb and Manalo-Smith, 2005; Zhang et al., 2005, Kaufman et al., 2005a, Matheson et al., 2005). Recently, Koren et al. (2007), using MODIS data, showed that the average reflectance for cloud-free ocean scenes far away from clouds were up to 30% lower than those near cloud edges. The higher reflectances lead to higher AOTs retrieved in the vicinity of clouds. This positive correlation can be explained as a result of physical phenomena such as the humidification of aerosols in the relatively moist cloud environment or a transition between aerosol and clouds where the cloud signature is weak (evaporation and/or activation of cloud drops) and the distinction between cloudy and cloud-free air becomes problematic. The term "twilight zone" was coined by Koren et al. (2007) to describe the regions around clouds which are neither precisely cloud-free nor precisely cloudy. On the other hand, part of the correlation can result from remote sensing artifacts such as cloud contamination of the cloud-free fields of view used in the aerosol retrievals. Kaufman and Koren (2006) noted that any "satellite analysis may be affected by potential cloud artifacts."

There are two ways that clouds affect the retrievals of aerosols: (*i*) the existence of small amounts of sub-pixel sized clouds in pixels identified as being cloud-free and (*ii*) an enhancement in the illumination of the cloud-free column through the reflection of sunlight by nearby clouds. When the pixels are relatively large (e.g., TOMS ~ 40 km, OMI ~ 15 km), only the first type (unresolved variability), cloud contamination is considered (e.g., Torres et al., 2002; Sinyuk et al., 2003). The second type (resolved variability), also called the 'cloud adjacency effect,' is more pronounced when satellite pixels are relatively small (e.g., MODIS and MISR ~ 0.5 km). Kobayashi et al. (2000), Cahalan et al. (2001), Podgorny (2003), Wen et al., (2001, 2006, 2007), Nikolaeva et al. (2005) studied the cloud adjacency effect when cloud-free pixels are brightened (or shadowed) by reflected light from surrounding clouds using 3D radiative transfer calculations applied to LANDSAT, MODIS, and ASTER data as well as to numerically generated cloud fields including an isolated cubical cloud. Both cloud contamination and the cloud adjacency effect may substantially increase reflected radiation and thus lead to

significant overestimates of the AOT. These two types of cloud effects, however, have different impacts on the retrieved AOT: sub-pixel clouds increase AOT by increasing the apparent contribution due to large particles (aerosol "coarse" mode), cloud adjacency mostly increases the apparent contribution due to small particles (aerosol "fine" mode). This short paper quantifies the second factor by using a simple stochastic cloud model to obtain the radiative flux reflected by broken clouds and comparing this flux with that obtained with the molecules in the atmosphere causing extinction, but no scattering.

The next section discusses the factors that contribute to the enhancement of a cloud-free column through the cloud adjacency effect. Section 3 introduces a simple two-layer model of the cloud enhancement with broken clouds as the lower layer and molecular scattering as the upper layer. A Poisson stochastic cloud model used to obtain the upward flux reflected by broken clouds is briefly described in Section 4. Section 5 compares the results of this simple model with those obtained from Monte Carlo calculations for broken cumulus clouds over Brazil observed by MODIS. Finally, Section 6 summarizes the results and discusses their implications.

2. Cloud enhancement and its contributors

Current methods used to retrieve AOT in cloud-free pixels account for sunlight reflected by the underlying surface and by the Rayleigh scattering due to molecules in the atmosphere but not the sunlight reflected by surrounding clouds. Sunlight reflected by the surrounding clouds, however, is an additional source of radiation that reaches the sensor as a result of (*i*) reflection by the underlying surface, (*ii*) scattering by the aerosol, and (*iii*) scattering by molecules. The relative roles of these three contributions varies from scene to scene and depends on many factors, including wavelength, surface reflectance, nearest cloud distance, cloud optical depth, the vertical and horizontal distributions of clouds, AOT, the vertical distribution of aerosols (relative to clouds), the solar and satellite viewing angles.

Wen et al. (2006, 2007) gained insight into the cloud adjacency effect by performing synthesized aerosol retrievals in realistic broken cumulus fields over a biomass burning region in Brazil as observed by MODIS. They assumed that all aerosols were below the cloud tops and used 3D and 1D radiative transfer calculations to

107 determine the average difference between the 3D and 1D reflectances for all cloud-free
108 pixels as given by

109 $$\Delta\rho = \overline{r_{3D}(x,y) - r_{1D}}\,. \qquad (1)$$

110 The calculations were performed for a variety of surface albedos and 3 different AOTs,
111 0.1, 0.5 and 1.0 at different wavelengths. They referred to $\Delta\rho$ as the 'cloud-induced
112 enhancement' or just 'cloud enhancement.' Figure 1 illustrates the results calculated for
113 the 0.47 μm wavelength. For dark surfaces the enhancement is not sensitive to AOT.
114 For bright surfaces, the enhancement decreases with AOT because the aerosol layer
115 prevents photons reflected by the surface from reaching the satellite. The intercept with
116 the vertical axis gives the enhancement for zero surface albedo and thus provides
117 estimates for the contribution from Rayleigh scattering. The contribution from molecular
118 scattering dominates over aerosol scattering which, as is evident from the figure, is nearly
119 an order of magnitude smaller even for an AOT of 1. The relative roles of molecular and
120 aerosol scattering arise because the scattering angles encountered in the retrievals of
121 aerosol properties are typically between 100° and 150°. For this the range of angles the
122 normalized phase functions for aerosols are much smaller than the Rayleigh phase
123 function (e.g., Liou, 2002, p. 98).

124 In summary, for dark surfaces and low-level clouds with aerosols below the cloud
125 layer, sunlight reflected by the clouds and then scattered by molecules in the cloud-free
126 columns is the key process for the enhancement of retrieved AOT, at least for the shorter
127 wavelengths at which Rayleigh scattering is strong. Since the enhancement is due
128 primarily to Rayleigh scattering and not very sensitive to AOT, the enhancement can be
129 assessed knowing only the cloud properties and the (average) distance from a cloud-free
130 pixel to a cloudy pixel.
131
132 **3. A simple model for the cloud-induced enhancement of reflectances for nearby**
133 **cloud-free columns**

134 Assume that the enhancement of the reflectance in the cloud-free column is due
135 *entirely* to Rayleigh scattering. Consider a simple, two-layer model with broken clouds
136 in the lower layer and a layer of molecules for the upper layer (Fig. 2). Take the cloud
137 enhancement to be the difference between the following two radiances: (a) one is

reflected from a broken cloud field with a scattering Rayleigh layer above it and (b) one is reflected from the same broken cloud field but with the molecules in the upper layer causing extinction, but no scattering. In other words,

$$\Delta\rho = r_1 - r_2 \tag{2}$$

where

$$r_1(\theta_0,\theta) = R_m(\theta_0,\theta) + \frac{\alpha_c(\tau,\theta_0)T_m(\theta_0)t_m(dif,\theta)}{1-\alpha_c(\tau,\theta_0)R_m(dif)} \tag{3}$$

and

$$r_2(\theta_0,\theta) = R_m(\theta_0,\theta) + \alpha_c(\tau,\theta_0)T_m(\theta_0)t_m(dif,\theta). \tag{4}$$

Here sub-index 'm' stands for 'molecule' while 'c' stands for 'cloud.' $R_m(\theta_0,\theta)$ is the reflectance for a molecular layer with no clouds below (this term is irrelevant here since it is canceled in calculating $\Delta\rho$). Cloud reflectance, α_c, is the critical parameter in this simple model because, in addition to cloud optical depth, τ, and SZA, θ_0, it is also a function of the cloud brokenness as will be discussed below. T_m is the transmittance through the molecular layer with direct sunlight incident from above while t_m is the transmission through the molecular layer for diffuse illumination from below. Finally, $R_m(dif)$ is the reflectance of the molecular layer illuminated by diffuse radiation from below. Note that with the exception of α_c, all the quantities in (2)-(4) are 1D and are calculated using a standard plane-parallel radiative transfer code. For simplicity, the surface is assumed to be black. Contributions from non-zero surface reflectances can be readily included in α_c.

In summary, a simple two-layer model with a broken cloud field below and Rayleigh scattering molecular layer above is used to quantify the cloud-induced enhancement of Rayleigh scattering. The enhancement comes from the enhanced illumination of the molecular layer through the reflection of sunlight by the surrounding clouds. The main unknown is the reflectance for a broken cloud field. If we assume that the clouds are plane-parallel rather than broken then α_c will be overestimated. Since $\Delta\rho$ in (2)-(4) is an increasing function with respect to α_c (Fig. 3), the plane-parallel approximation will also overestimate the effect of clouds on cloud-free pixels.

166 The next section will describe the calculation of α_c for a broken cloud field using
167 a stochastic model. The advantage of using a stochastic model is that the output is
168 'generic.' It is averaged over many realizations of a cloud field with given statistical
169 properties.
170
171 **4. The Poisson stochastic model for broken clouds**
172 The one-layer Poisson model for broken clouds originally proposed by Titov
173 (1991) is used to calculate the cloud reflectance for broken cloudy regions. Kassianov
174 (2003) generalized this one-layer model to multilayer broken cloud fields while
175 Zhuravleva and Marshak (2005) validated the one-layer model by comparing results with
176 those generated using fractal cloud fields. The main parameters in the model are as
177 follows: (*i*) cloud fraction, A_c, (*ii*) averaged cloud optical depth τ, and (*iii*) cloud aspect
178 ratio, γ, which is defined as the ratio of cloud vertical to horizontal dimensions. In
179 addition, the single scattering albedo and the cloud droplet scattering phase function
180 along with the surface albedo are specified. For the shortwave calculations performed
181 here, the droplet single-scattering albedo is set to unity and the C1 phase function
182 (Deirmendjian, 1969) was used. Figure 4 shows an example of two broken cloud fields
183 with $A_c = 0.3$ and $\gamma = 0.5$ and 1.
184 The output of the stochastic model is the domain (and ensemble) averaged upward
185 and downward fluxes with downward fluxes subdivided into diffuse and direct
186 components. Zhuravleva and Marshak (2005) used these subdivided fluxes to determine
187 cloud aspect ratios from ground-based measurements.
188 Note that two (averaged cloud optical depth, τ, and cloud fraction, A_c) out of the
189 three principal input parameters can be determined from the MODIS Cloud Product
190 (MOD06). The third parameter (cloud aspect ratio γ) is not readily available.
191 Fortunately, as is shown in the next section, the cloud enhancement is not very sensitive
192 to the aspect ratio, at least for small solar zenith angles.
193 A simple one-layer stochastic model is used to derive cloud reflectances as a
194 function of the average cloud optical depth, cloud fraction, and cloud aspect ratio for
195 broken cloud regions. The clouds are distributed in space according to a Poisson

196 distribution so that the average distance from a cloud-free pixel to a cloud edge is
197 uniquely determined by cloud fraction and cloud aspect ratio.
198
199 **5. Results**
200 Figure 5 shows the cloud-induced enhancement $\Delta\rho$ as a function of cloud optical
201 depth for 0.47 μm and four cloud fractions: A_c = 1.0, 0.7, 0.5, and 0.3. The aspect ratio
202 γ= 1, the solar zenith angle θ_0 = 60°, the view zenith angle θ = 0°, and the surface
203 albedo, α_s = 0.0. Note that the case of A_c = 1.0 represents unbroken clouds and
204 corresponds to the plane-parallel approximation. The figure depicts an example of a
205 look-up-table (LUT) that can be used to estimate the expected enhancement of cloud-free
206 radiances in the vicinity of clouds. Consider a broken cloud scene with 70% cloud cover
207 and an average cloud optical depth of 22 illuminated by the sun with a zenith angle of
208 60°. The enhancement in Rayleigh scattering at 0.47 μm in the nadir direction will likely
209 be 0.04 larger than its 1D counterpart.
210 To assess the merits of the above approach, estimates of the cloud enhancement
211 were made for the two 68 by 80 km broken cloud scenes in biomass-burning regions of
212 Brazil studied by Wen et al. (2007). Both scenes were simultaneously observed by
213 MODIS and ASTER. The first cloud scene (centered at 0.0N, 53.78W and acquired on
214 Jan. 25, 2003) was described by Wen et al. (2006) while the retrieved cloud parameters
215 for the second scene (centered at 17.1S, 42.16W and acquired on Aug. 9, 2001) were
216 described and analyzed by Marshak et al. (2006).
217 The first scene had cloud fraction A_c = 0.53 and cloud optical depth τ= 12 (std =
218 10), and the solar zenith angle was θ_0 = 32°. The surface was covered by vegetation with
219 a low albedo of 0.011 at 0.47 μm and 0.025 at 0.65 μm. For this scene, Wen et al. (2007)
220 found an average cloud enhancement of 0.015 (std = 0.005) at 0.47 μm and 0.004 (std =
221 0.008) at 0.65 μm (marked as 'squares' in the left panel of Fig. 6). Two 15 by 15 km
222 subsets of this scene with thick (τ= 14, std = 8, and A_c = 0.59) and thin (τ= 7, std = 6, and
223 A_c = 0.51) broken clouds were also examined using high-resolution cloud fields retrieved
224 from ASTER data in 3D Monte Carlo simulations of the radiance fields. The cloud-

induced enhancement was found to be 0.019 and 0.012 at 0.47 μm for thick and thin clouds and 0.01 and 0.0018 at 0.65 μm (marked as 'circles' in the left panel of Fig. 6). In addition, Fig. 6 shows asymptotic values (marked as 'ovals' in the left panel of Fig. 6) corresponding to the enhancements at the largest distances from cloud edges. At the greatest distances from the clouds, cloud shadows are generally avoided thereby giving a more representative estimate of the 3D effects than that obtained by averaging over all of the cloud-free pixels, some being darkened by shadows.

The second scene had cloud fraction, $A_c = 0.4$ and cloud optical depth, $\tau = 8$ (std = 8) and solar zenith angle, $\theta_0 = 41^\circ$ (right panel of Fig. 6). The surface was much more heterogeneous than the surface for the first scene. It was also much brighter at shorter wavelengths with an average albedo of 0.04 at 0.47 μm, 0.07 at 0.65 μm (and 0.2 at 0.84 μm.) For this scene, Wen et al. (2007) found an asymptotic cloud enhancement of 0.006 at 0.47 μm and 0.003 at 0.66 μm ('ovals') at a distance of about 3 km from the cloud edges. The average values ('squares') for the cloud-free pixels selected by the MODIS AOT retrieval algorithm (Remer et al., 2005) have been included.

As the results in Fig. 6 indicate, the estimates based on the stochastic model can serve as a good first-order approximation to the cloud-induced enhancement calculated with a Monte Carlo code. The stochastic model underestimates somewhat the enhancement, at least for the particular scenes studied. Clearly, the enhancement is much smaller than would be obtained with a plane-parallel approximation ($A_c = 1$).

The left panel of Fig. 6 also illustrates the sensitivity of the modeled cloud enhancement, $\Delta\rho$, to cloud aspect ratio. For three wavelengths (0.47, 0.65, and 0.84 μm) and cloud fraction $A_c = 0.6$ the cloud enhancement as a function of optical depth τ is given for three cloud aspect ratios: $\gamma = 0.5, 1, 2$. For a fixed cloud geometrical thickness of 1 km, this means that the average cloud horizontal dimension varies from 500 m to 2 km. The uncertainties caused by an unknown (but reasonable) aspect ratio are of the order of 5-10%. For small cloud fractions and large solar zenith angles the modeled enhancements become more sensitive to cloud aspect ratio.

The right panel of Fig. 6 also shows the effect of surface albedo. For small cloud fraction the contribution of a bright surface to the total cloud-induced enhancement can

255 be significant. It is interesting to note that, in contrast to plane-parallel clouds, the
256 surface contribution to the total enhancement does not decrease with cloud optical depth.
257 It is almost constant. This is a special feature of broken cloud fields where the radiation
258 reflected by the surface in cloud-free regions goes directly to a satellite detector rather
259 than being attenuated by the clouds.

260 Finally, the effect of the enhancement on the Angström exponent in the vicinity of
261 clouds is studied. The Angström exponent characterizes the dependency of aerosol
262 optical thickness on wavelength and is related to the average size of the particles in the
263 aerosol: the smaller the particles, the larger the exponent.

264 Consider three cases with the "true" Angström exponents equal to 0 for a "clean"
265 environment, 1.04 for a "polluted" environment, and 2.14 for a "very polluted"
266 environment for 0.47 and 0.65 μm, and 0, 1.31, and 2.7 for 0.65 and 0.84 μm. The clean
267 case with zero Angström exponent indicates that the extinction is independent of
268 wavelength, as it is for clouds and for large nonabsorbing aerosols, like sea salt. The
269 AOT is taken to be 0.1 at 0.65 μm. Taking into account the cloud-induced enhancement,
270 the "apparent" Angström exponent will be greater than zero. Figure 7 illustrates the
271 increase in Angström exponents for both spectral intervals. Obviously, for highly
272 polluted environments, the cloud adjacency effect is much smaller than for clean
273 environments. Nonetheless, owing to the effects of clouds, the retrieved Angström
274 exponent can be substantially larger than its true value. The cloud adjacency effect is
275 opposite that for cloud contamination where subpixel scale clouds increase the "coarse"
276 mode fraction thereby decreasing the Angström exponent.
277
278 **6. Summary and discussion**

279 A simple model was described for estimating the cloud-induced enhanced
280 reflectances of cloud-free columns in the vicinity of clouds. The enhancement was
281 assumed to be due entirely to Rayleigh scattering. For the shorter wavelengths where
282 molecular scattering is relatively large, attributing the enhancement to the illumination of
283 the Rayleigh scattering atmosphere by sunlight reflected from nearby clouds proved
284 reasonable (Fig. 1) for scenes with dark surfaces, broken, low-level cumulus clouds, and

285 an aerosol layer below the cloud tops. The enhancement in Rayleigh scattering was
286 estimated using a stochastic cloud model (Fig. 4) to obtain the radiative flux reflected by
287 broken clouds and comparing this flux with that obtained with the molecules in the
288 atmosphere causing extinction, but no scattering as given by (2)-(4).

289 The results of numerical simulations of the enhancement (Wen et al. 2007) were
290 shown to be in good agreement (Fig. 6) with the simple model, although the model
291 underestimates somewhat the enhancement for the particular scenes studied, cumulus
292 cloud fields retrieved from collocated MODIS and ASTER images over a biomass
293 burning region in Brazil.

294 The one-layer Poisson stochastic cloud model (Titov, 1990) uses cloud optical
295 depth, τ, droplet single scattering albedo and scattering phase function, cloud fraction,
296 A_c, cloud aspect ratio, γ, and surface albedo to estimate reflectances for broken cloud
297 fields. The optical depth and cloud fraction are given in the MODIS Cloud Product
298 (MOD06). They can be used as a first approximation to quantify the cloud-induced
299 enhancement from precalculated look-up-tables (see Fig. 5, for an example). The cloud
300 aspect ratio is not readily available but the error due to an incorrect cloud aspect ratio is
301 5-20%. For clouds distributed in space according to a Poisson distribution, the average
302 distance from a cloud-free pixel to the nearest cloud is uniquely determined by cloud
303 fraction and cloud aspect ratio.

304 The assumption that the enhancement of the cloud-free column is due to molecular
305 scattering leads naturally to a larger increase of AOT for shorter wavelengths, or to a
306 "bluing" of aerosols near clouds (Fig. 7). As a result, in contrast to cloud contamination
307 by sub-pixel clouds, the cloud adjacency effect will increase the apparent aerosol "fine"
308 mode fraction rather than the "coarse" mode fraction. Recent findings in the MODIS
309 cloud and aerosol products indicate that the AOT and its fine mode fraction increase in
310 the vicinity of clouds (Kaufman et al., 2005b).

311 Since MODIS and CERES are on the same spacecraft, another approach to
312 estimating spectral upward fluxes for broken cloud fields is to use the CERES data.
313 Using CERES fluxes rather than a stochastic cloud model requires the use of a theoretical
314 radiative transfer model to convert broadband fluxes to spectral fluxes. A simpler

approach would be to ignore the wavelength dependence in the anisotropy as given by the CERES Angular Distribution Models (ADMs) (Loeb et al. 2005) and use the ADMs to determine spectral fluxes from the MODIS radiances. This approach, however, can lead to the large errors at the 10 by10 km scale of the MODIS Aerosol Product and needs further study.

The enhanced illumination of cloud-free columns is a key part of characterizing aerosol properties in the vicinity of clouds. In satellite based studies of cloud-aerosol interactions, changes in the properties of the aerosol due to the cloud environment must be separated from the apparent changes that come from 3D cloud-radiative transfer effects on the retrieved aerosol properties.

The simple model presented here should be taken as limited to the case of low-level clouds over dark surfaces with the aerosol below the cloud tops. The model may well prove inappropriate for scenes with highly reflecting surfaces, with upper-level clouds, or in which a substantial fraction of the aerosol lies above the low-level clouds. In such cases molecular scattering will not necessarily have the dominant role that it has for the low-level cloud and aerosol systems studied here.

Acknowledgments. This work was supported by the Department of Energy (under grant DE-AI02-95ER61961 to NASA's GSFC) as part of the Atmospheric Radiation Measurement (ARM) program, and by NASA's Radiation Program Office (under grants 621-30-86 and 622-42-57). We thank C. Chiu, A. Davis, I. Koren, T. Varnai, and W. Wiscombe for stimulating discussions.

References

Cahalan, R. F., L. Oreopoulos, G. Wen, A. Marshak, S.-C. Tsay, and T. DeFelice, 2001: Cloud Characterization and Clear Sky Correction from Landsat 7. *Remote Sens. Environ.*, **78**, 83-98.

Deirmendjian, D., 1969: *Electromagnetic Scattering on Spherical Polydispersions.* Elsevier, New York (NY), 292 pp.

Kassianov E., 2003: Stochastic radiative transfer in multilayer broken clouds. Part I: markovian approach. *J. Quant. Spectrosc. Radiat. Transfer*, **77**, 373-394.

Kaufman, Y.J., L.A. Remer, D. Tanre, R.R. Li, R. Kleidman, S. Mattoo, R. Levy, T. Eck, B.N. Holben, C. Ichoku, J. Martins, and I. Koren, 2005a: A critical examination of the residual cloud contamination and diurnal sampling effects on MODIS estimates of aerosol over ocean. *IEEE Trans. Geosci. Remote Sens.*, **43**, 2886-2897.

Kaufman, Y. J., I. Koren, L. A. Remer, D. Rosenfeld, and Y. Rudich, 2005b: The effect of smoke, dust and pollution aerosol on shallow cloud development over the Atlantic ocean. *Proceedings of the National Academy of Sciences*, 10.1073/pnas.0505191102.

Kaufman, Y.J., and I. Koren, 2006: Smoke and pollution aerosol effect on cloud cover, *Science*, **313**, 655-658.

Kobayashi T., K. Masuda, M. Sasaki, J. Mueller, 2000: Monte Carlo simulations of enhanced visible radiance in clear-air satellite fields of view near clouds. *J. Geophys. Res.*, **105**, 26569-26576.

Koren, I., L. A. Remer, Y. J. Kaufman, Y. Rudich, and J. V. Martins, 2007: On the twilight zone between clouds and aerosols. *Geophys. Res. Lett.*, **34**, L08805, doi:10.1029/2007GL029253.

Liou, K. N., 2002: An introduction to atmospheric radiation. Academic Press, New York, 583 pp.

Loeb, N. G., and N. Manalo-Smith, 2005: Top-of-atmosphere direct radiative effect of aerosols over global oceans from merged CERES and MODIS observations. *J. Climate*, **18**, 3506-3526.

Loeb, N. G., S. Kato, K. Loukachine, and N. M. Smith, 2005: Angular distribution models for top-of-atmosphere radiative flux estimation from the Clouds and the Earth's Radiant Energy System instrument on the *Terra* satellite. Part I: Methodology. *J. Atmos. Oceanic Technol.*, **22,** 338–351.

Matheson, M.A., J.A. Coakley, Jr., and W.R. Tahnk, 2005: Aerosol and cloud property relationships for summertime stratiform clouds in the northeastern Atlantic from AVHRR observations. *J. Geophys. Res.*, **110,** D24204, doi:10.1029/2005JD006165.

Marshak, A., S. Platnick, T. Varnai, G. Wen, and R. F. Cahalan, 2006: Impact of 3D radiative effects on satellite retrievals of cloud droplet sizes, *J. Geophys. Res.*, **111**, DO9207, doi:10.1029/2005JD006686.

377 Nikolaeva, O.V., L. P. Bass, T. A. Germogenova, A. A. Kokhanovisky, V. S. Kuznetsov,
378 and B. Mayer, 2005: The influence of neighboring clouds on the clear sky
379 reflectance with the 3-D transport code RADUGA, *J. Quant. Spectrosc. Radiat.*
380 *Transf.*, **94**, 405–424.

381 Podgorny, I.A., 2003: Three-dimensional radiative interactions in a polluted broken
382 cloud system. *Geophys. Res. Lett.*, **30**, 1771, doi:10.1029/2003GL017287.

383 Remer, L. A., and 12 other coauthors, 2005: The MODIS aerosol algorithm, products,
384 and validation, *J. Atmos. Sci.*, **62**, 947-973.

385 Sekiguchi, M., T. Nakajima, K. Suzuki, K. Kawamoto, A. Higurashi, D. Rosenfeld, I.
386 Sano, S. Mukai, 2003: A study of the direct and indirect effects of aerosols using
387 global satellite data sets of aerosol and cloud parameters. *J. Geophys. Res.*,
388 **108**(D22), 4699, doi:10.1029/2002JD003359.

389 Sinyuk A., O. Torres, and O. Dubovik, Imaginary refractive index of desert dust using
390 satellite and surface observations, 2003: *Geophys. Res. Letters,* **30** (2), 1081, doi:
391 10.1029/2002GL016189.

392 Titov, G. A., 1990: Statistical description of radiation transfer in clouds. *J. Atmos. Sci.*,
393 **47**, 24–38.

394 Torres, O., P.K. Bhartia, J.R. Herman, A. Syniuk, P. Ginoux, and B. Holben, 2002: A
395 long term record of aerosol optical depth from TOMS observations and comparison
396 to AERONET measurements, *J. Atm. Sci.,* **59**, 398-413.

397 Wen, G., R. F. Cahalan, T.-S. Tsay, and L. Oreopoulos, 2001: Impact of cumulus cloud
398 spacing on Landsat atmospheric correction and aerosol retrieval. *J. Geophys. Res.*,
399 **106**, 12129-12138.

400 Wen, G., A. Marshak, and R. F. Cahalan, 2006: Impact of 3D clouds on clear sky
401 reflectance and aerosol retrievals in biomass burning region of Brazil. *Geosci.*
402 *Remote Sens. Lett.,* **3**, 169-172.

403 Wen, G., A. Marshak, and R. F. Cahalan, L. A. Remer, and R. G. Kleidman, 2007: 3D
404 aerosol-cloud radiative interaction observed in collocated MODIS and ASTER
405 images of cumulus cloud fields. *J. Geophys. Res.,* **23**, xxxx, doi:
406 10.1029/2006JD008267.

407 Zhang, J., J. S. Reid, B. N. Holben, 2005: An analysis of potential cloud artifacts in
408 MODIS over ocean aerosol optical thickness product. *Geophys. Res. Lett.,* **32**,
409 10.1029/2005GL023254.

410 Zhuravleva, T., and A. Marshak, 2005: On the validation of the Poisson model of broken
411 clouds. *Izvestiya Atmos. and Oceanic Phys.*, **41**, 6, 713-725.

412

412 **Figures**

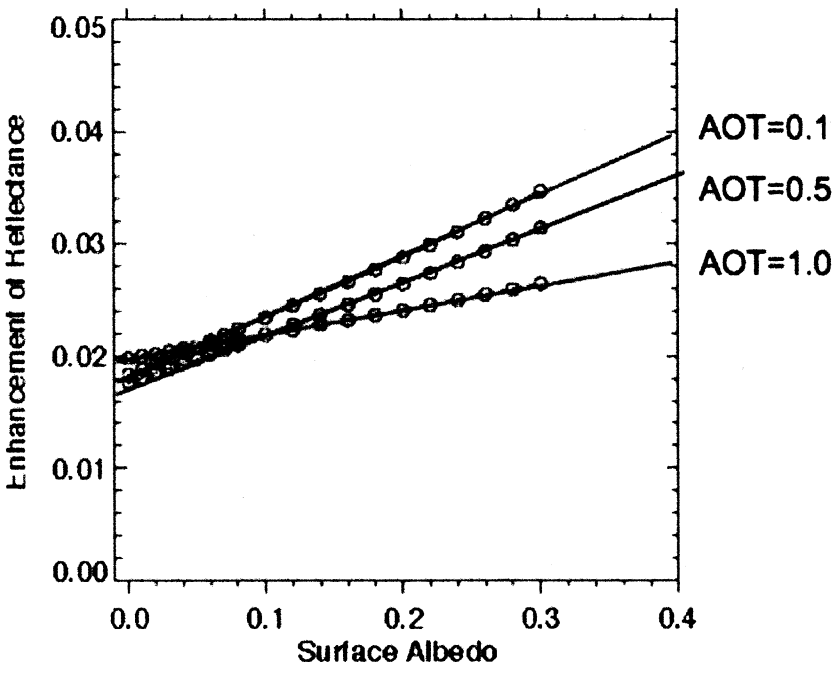

413

414 **Figure 1**. Cloud-induced enhancement as a function of surface albedo and AOT for a
415 broken cumulus scene with cloud cover close to 50% described in Wen et al. (2007). The
416 Rayleigh scattering is for 0.47 μm.
417

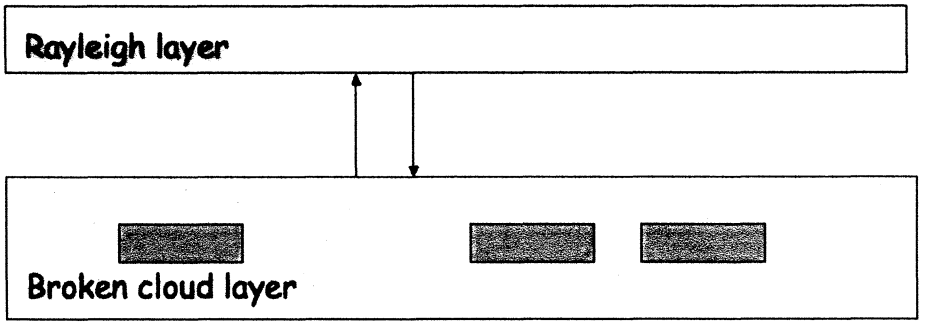

417

418 **Figure 2.** A schematic two-layer model of a broken cloud field (lower layer) and
419 Rayleigh scatterers (upper layer).
420

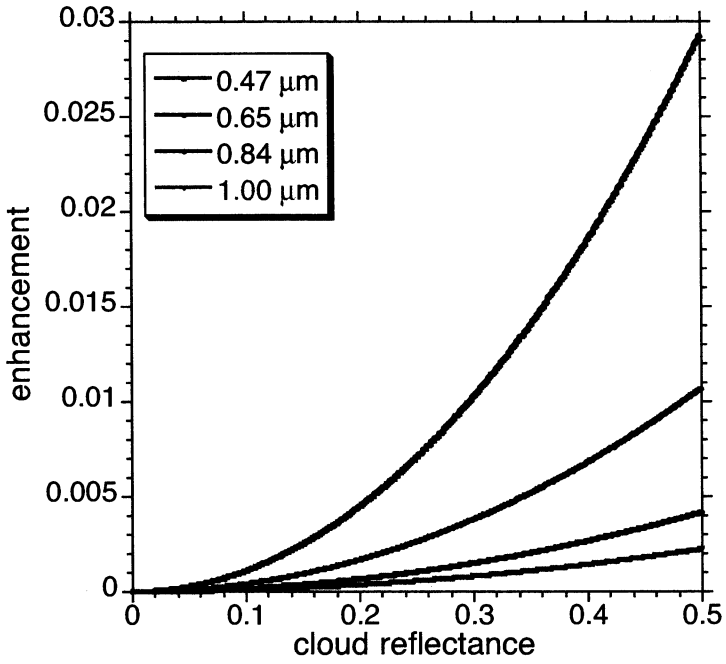

Figure 3. Cloud-induced enhancement as a function of cloud reflectance for four wavelengths: 0.47, 0.65, 0.84, and 1.00 μm. The Rayleigh optical depth is taken to be 0.05 at 0.65 μm and varies inversely with the fourth power of the wavelength. The solar zenith angle, $\theta_0 = 60^\circ$, viewing zenith angle $\theta = 0^\circ$, and the surface is black.

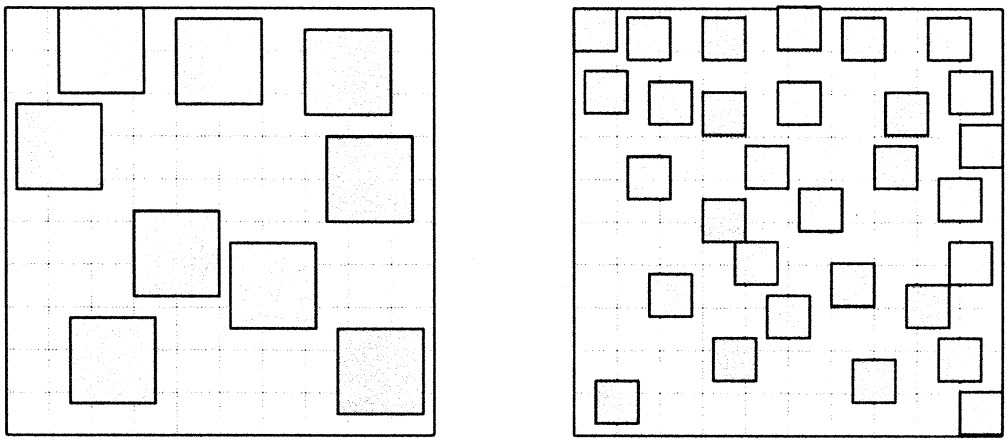

426

427 **Figure 4**. An example of the Poisson distribution of broken cloud fields with cloud
428 fraction $A_c = 0.3$ for a 10 by 10 km area. For a cloud vertical thickness of 1 km, the left
429 panel has cloud aspect ratio $\gamma = 0.5$, and the right panel has $\gamma = 1$.

430

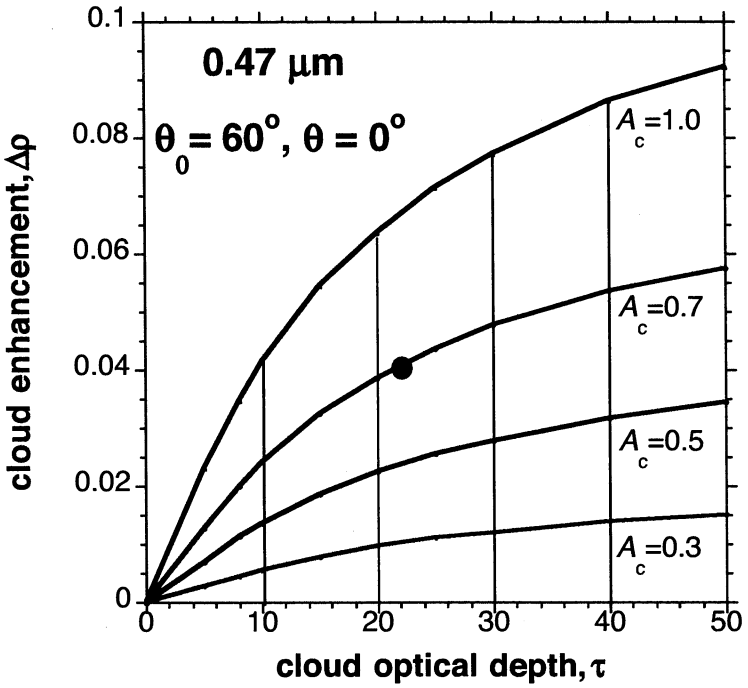

Figure 5. Cloud-induced enhancement $\Delta\rho$ and cloud optical depth τ for four cloud fractions, A_c = 1.0, 0.7, 0.5, and 0.3. A_c = 1 corresponds to the plane-parallel approximation. The aspect ratio is γ= 1, solar zenith angle, θ_0 = 60°, view zenith angle, θ = 0°, and the surface is black. The filled circle indicates the expected cloud-free radiance enhancement due to nearby clouds with τ =22 and A_c = 0.7.

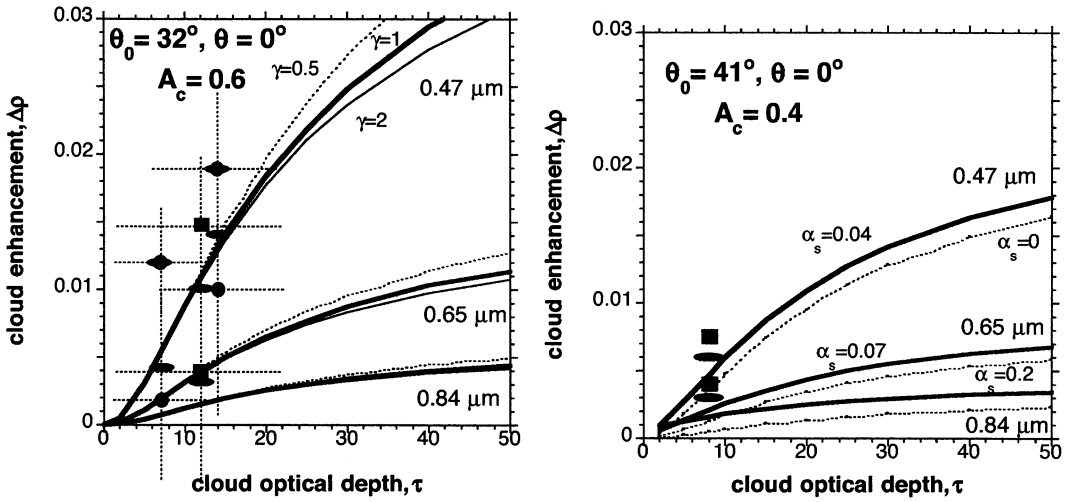

436

437 **Figure 6**. Cloud-induced enhancement $\Delta\rho$ and cloud optical depth, τ, for three
438 wavelengths: 0.47, 0.65, and 0.84 μm. (**Left**) Cloud fraction, $A_c = 0.6$, solar zenith angle,
439 $\theta_0 = 32°$, and view zenith angle, $\theta = 0°$. These conditions correspond to the first broken
440 Cu scene studied by Wen et al. (2007). Thick solid lines are $\Delta\rho$ calculated using (2)-(4)
441 with aspect ratio $\gamma = 1$, dotted lines are with $\gamma = 2$, and thin solid lines with $\gamma = 0.5$. The
442 surface is black. Filled blue and red squares, circles and ovals are from Wen et al. (2007)
443 at 0.47 and 0.66 μm. Squares correspond to the scene average values; circles correspond
444 to two subscenes with thick and thin clouds, and ovals correspond to asymptotic values.
445 The dotted lines coursing through the symbols give one standard deviation. (**Right**)
446 Cloud fraction, $A_c = 0.4$, solar zenith angle, $\theta_0 = 41°$, and view zenith angle, $\theta = 0°$.
447 These conditions correspond to the second broken Cu scene studied by Wen et al. (2007)
448 and by Marshak et al. (2006). The aspect ratio $\gamma = 1$. Dotted lines are $\Delta\rho$ calculated using
449 (2)-(4) for a black surface. Solid lines are for the $\Delta\rho$ that correspond to the MODIS-
450 retrieved surface spectral albedos: $\alpha_s = 0.04$ at 0.47 μm, $\alpha_s = 0.07$ at 0.65 μm, and $\alpha_s = 0.2$
451 at 0.84 μm. Filled ovals and squares are also from Wen et al. (2007). Ovals correspond
452 to the actual asymptotic values while squares are the average enhancements for those
453 pixels that were selected by the MODIS AOT retrieval algorithm (see text for details).
454

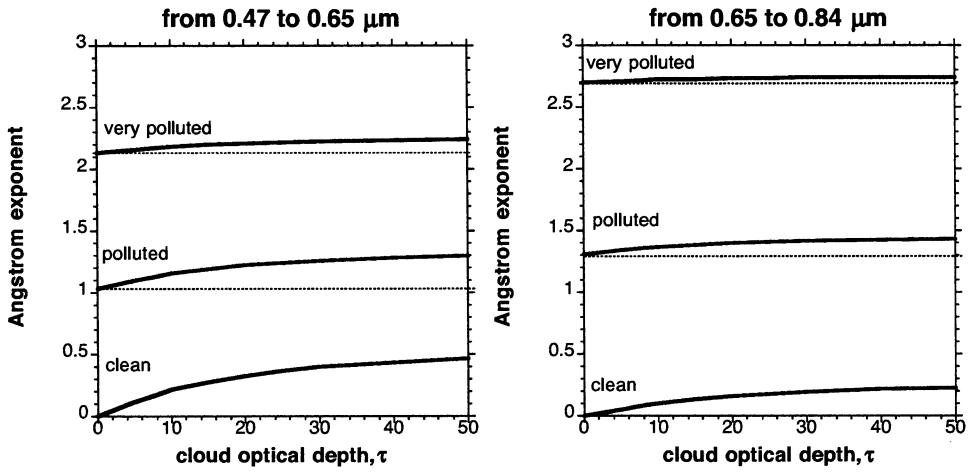

Figure 7. The Angström exponent and cloud optical depth, τ, for three situations: "clean," "polluted," and "very polluted." The cloud fraction is $A_c = 0.5$, the aspect ratio, $\gamma = 0.5$, and the illumination and viewing directions are the same as in Fig. 5. Two spectral intervals are shown: **left** panel is for 0.47 and 0.65 μm while **right** panel is for 0.65 and 0.84 μm.